Computers in Biology and Medicine 114 (2019) 103476

Contents lists available at ScienceDirect

Computers in Biology and Medicine

journal homepage: http://www.elsevier.com/locate/compbiomed

Comparison of magnetic field distributions generated by various permanent magnets for transcranial static magnetic stimulation: A simulation study

Jimin Park [a], Chany Lee [b], Sangjun Lee [a], Chang-Hwan Im [a,*]

[a] Department of Biomedical Engineering, Hanyang University, Seoul, Republic of Korea
[b] Department of Structure & Function of Neural Network, Korea Brain Research Institute, Daegu, Republic of Korea

ARTICLE INFO

Keywords:
Transcranial static magnetic stimulation (tSMS)
Finite element method (FEM)
Magnetic flux density
Permanent magnets
Noninvasive brain stimulation

ABSTRACT

Recent experimental studies have shown that static magnetic field can be effective in modulating human brain functions. Following this discovery, a new noninvasive brain stimulation technique was developed: the transcranial static magnetic stimulation (tSMS). Various types of permanent magnets have been used in previous experimental studies, with the aim of validating the effectiveness of tSMS; nevertheless, the spatial distributions of magnetic field generated by these permanent magnets have not been fully investigated. In this study, we compared the distributions of magnetic field on the human cortical surface generated by five different cylindrical magnets (of various dimensions), using the finite element method. Our simulation results demonstrated that the magnitude of magnetic flux density induced in the cortical grey matter of the human brain is proportional to the volume of permanent magnets used, while the magnetic field gradient is not necessarily proportional to the volume of the magnets. Additionally, we showed that the use of magnets with internal holes might not be advantageous. The differences in magnetic field properties induced by various types of permanent magnets suggested that their careful selection, based on magnetic field simulations, might be necessary to increase the effectiveness of tSMS.

1. Introduction

Noninvasive electromagnetic brain stimulation techniques (i.e., transcranial magnetic stimulation (TMS) and transcranial direct current stimulation (tDCS)) have attracted increasing interest from neuroscientists, especially due to their potential in clinical applications. It has been documented that both TMS and tDCS can alter cortical excitability through the application of weak currents to cortical neurons, thereby modulating various human brain functions noninvasively. Recently, it has been shown that also a static magnetic field (SMF) can alter cortical excitability in humans [1] as well as non-primate animals [2,3]. This relatively new noninvasive brain stimulation technique is called transcranial static magnetic stimulation (tSMS). Following a first study, reporting the inhibitory effect of tSMS on the human motor cortex [1,4,5], further research has shown that tSMS is effective in modulating various brain areas (e.g., the supplementary motor cortex [6], the visual cortex [7,8], the sensorimotor cortex [9], the primary somatosensory cortex [10], temporal cortex [11] and the cerebellum [12]). Several issues, regarding the safety of tSMS and the proper selection of permanent magnets, have been also addressed [13,14].

Previous studies on tSMS, consistently reported reduced cortical excitability in healthy subjects, regardless of the polarity of the permanent magnets. The most plausible explanation for this phenomenon is that tSMS might alter the functions of membrane ion channels at cellular level [15], due to the diamagnetic anisotropy of phospholipids. Other hypothetical mechanisms for elucidating the working mechanisms of tSMS include: the alteration of activation kinetics of voltage-gated channels due to deformation [16], and the forcing of diamagnetic calcium ions away from a strongly interconnected astrocyte network, operated by the magnetic gradient [1]. Despite the efforts to explain this phenomenon in previous studies [1,15–17], it is still unclear whether it's stronger magnetic flux density or gradient that influences more on the efficacy of tSMS.

The simulation of the magnetic field distribution generated by tSMS can help to understand the underlying mechanisms of tSMS; however, so far, only one simulation study has been conducted using the finite element method (FEM) to analyze the flux density distributions generated by a permanent magnet [18]. In that study, the magnetic field properties such as field intensity, gradient, and focality at multiple locations, produced by a cylindrical permanent magnet

* Corresponding author.
E-mail addresses: jiminpark0805@gmail.com (J. Park), chan0511@hanmail.net (C. Lee), sangjunlee35@gmail.com (S. Lee), ich@hanyang.ac.kr (C.-H. Im).

https://doi.org/10.1016/j.compbiomed.2019.103476
Received 15 April 2019; Received in revised form 8 September 2019; Accepted 27 September 2019
Available online 28 September 2019

(diameter = 5.08 cm, height = 2.54 cm) were simulated using a human head model. The aforementioned permanent magnet has not been the only effective magnet in experimental studies. Indeed, several permanent magnets, with variable dimensions and properties, were used in previous experimental studies [1,12,14]: all of them had statistically meaningful effects. On the other hand, the usability of multiple permanent magnets with different properties has been tested experimentally [13], in an effort to provide tSMS hardware candidates; however, to the best of our knowledge, no studies have compared the magnetic field distributions generated by different permanent magnets. Here, we simulated various types of permanent magnets with the aim of finding potentially the best tSMS hardware settings, which might eventually lead to the most effective outcomes in practical applications. To achieve these goals, we first computed magnetic flux density and its gradient using FEM, when the coercive forces for neodymium magnets were evaluated based on the magnetic field measurement. Then, the magnetic field distributions generated by various types of neodymium magnets on the cortical surface of a realistic human head model were compared.

2. Methods

2.1. Finite element (FE) head model

A realistic head model was constructed from the MRI data of a 26-year-old healthy male subject. The T1-weighted MRI dataset was acquired using a 3T MAGNETOM Trio Scanner (Siemens, Erlangen, Germany; spatial resolution = 0.8 mm × 0.8 mm x 0.8 mm). Subvolumes of scalp, skull, grey matter, white matter, and cerebrospinal fluid (CSF) were segmented using an open software package called SimNIBS [19]; the segmented head model was then manually corrected using ITK-SNAP (www.itksnap.org). The final head model consisted of approximately 4.4 million tetrahedral elements. A cross-sectional view of the human head model is shown in Fig. 1.

2.2. Magnet model and magnetic flux density simulation

Four different permanent magnets (M30, M45, M60, and M60qr) were considered in this study [13]. The dimensions and properties of these permanent magnets are presented in Fig. 2 and Table 1. M60qr had an internal hole with different diameters on each side. The diameters of the internal holes were 6 mm on one side, and 16 mm on the other side. When a cylindrical base with a 16-mm diameter hole was facing the scalp (Fig. 2d), the magnet was called M60qr16. When a cylindrical base with a 6-mm diameter hole was facing the scalp (Fig. 2e), the magnet was called M60qr6. The magnetic flux density generated by five different permanent magnets (M30, M45, M60, M60qr16, and M60qr6) were simulated using an axisymmetric finite element (FE) solver embedded in a software package FEMM (www.femm.info).

The FEMM software uses the 'current sheet model' to compute magnetic field generated by axisymmetric permanent magnets, for which an axisymmetric permanent magnet is assumed to be a ferromagnetic material surrounded by a thin sheet of current [20]. This model calculates magnetic flux density induced by a hypothetical surface current density. At an arbitrary coordinate P(P_r, P_z), where the origin is located at the center of a modeled cylindrical magnet, the magnetic flux density induced by a segment of the current sheet with unit length can be found by applying the Biot-Savart's law, as

$$\Delta \boldsymbol{B} = \frac{\mu_0 \boldsymbol{I} \Delta \boldsymbol{l} \times \boldsymbol{S}}{4\pi |\boldsymbol{S}|^3} \quad (1)$$

where $\boldsymbol{l}$, $\boldsymbol{S}$, and $\boldsymbol{B}$ represent a unit vector with the direction of current, a vector starting from the center of the segment to an arbitrary point P(P_r, P_z), and the magnetic flux density induced by the segment, respectively. The total magnetic flux density can be calculated by the integration of $\Delta \boldsymbol{B}$. Then, magnetic field properties of the given cylindrical magnets can be derived by calculating magnetomotive force (MMF) with the total magnetic flux density and matching the computed MMF value with the coercive force of the given material (Neodymium in this study).

The coercive forces of the permanent magnets were estimated by matching the measured and the simulated magnetic flux densities. The magnetic flux density of M60 (www.neurek.com, Neurek SL) was measured using a hall effect sensor (Teslameter WT10A, KAIST) with a dynamic range of 0–2000 mT and a basic error of 5%. The measurement points were located along the cylindrical axis of M60, at regular steps of 1 cm, from the center of the base up to 6 cm height from the center. Similar measurement data were obtained for the other magnets in a previous study [13]. With the estimated coercive force, the reliability of our simulation method (FEMM) was validated by comparing the analytic and numerical solutions. The analytic solution employed in this study provides approximated magnetic flux density along the axial axis [21], and therefore magnetic flux density values only along the axial axis were compared. The average error evaluated for six points (0–5 cm with a step size of 1 cm) was just 3.2 ± 4.2 mT, demonstrating the high accuracy of our numerical solver.

Changes in magnetic flux density along the cylindrical magnet axis (i.e., 'axial direction') and along the direction perpendicular to the cylindrical axis (i.e., 'radial direction') were observed in simulation. The axial measuring points were distributed from the center of each magnet base up to 5 cm height, at regular steps of 0.5 cm. The radial measurement points started at 1.57 cm height from the center of the magnet base, which corresponds to the distance between the magnet base and the cortical grey matter (right hand motor cortex) of the human head model. The radial measurement points were distributed at regular steps of 0.5 cm, up to 5 cm from the central axis. The gradients of magnetic flux density were calculated at each given point: the measuring point was displaced by 1 mm in each direction. The magnetic field quantities

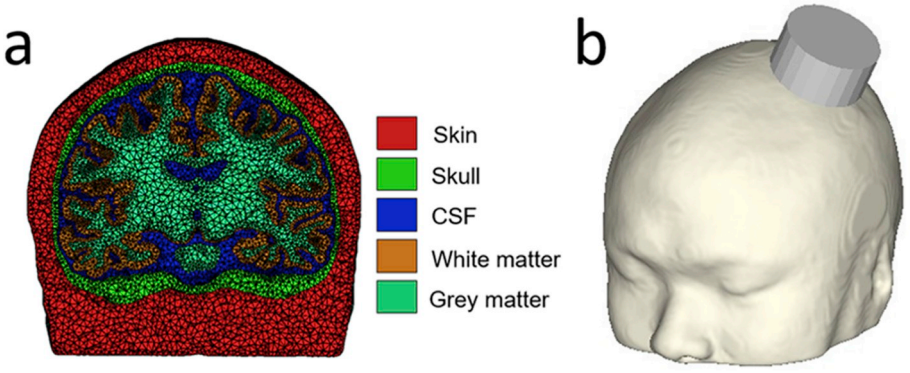

Fig. 1. Finite element head model constructed using the MRI data: Cross-sectional view of the realistic human head model (**a**), M60 magnet placed on the scalp, above the left primary motor cortex (**b**).

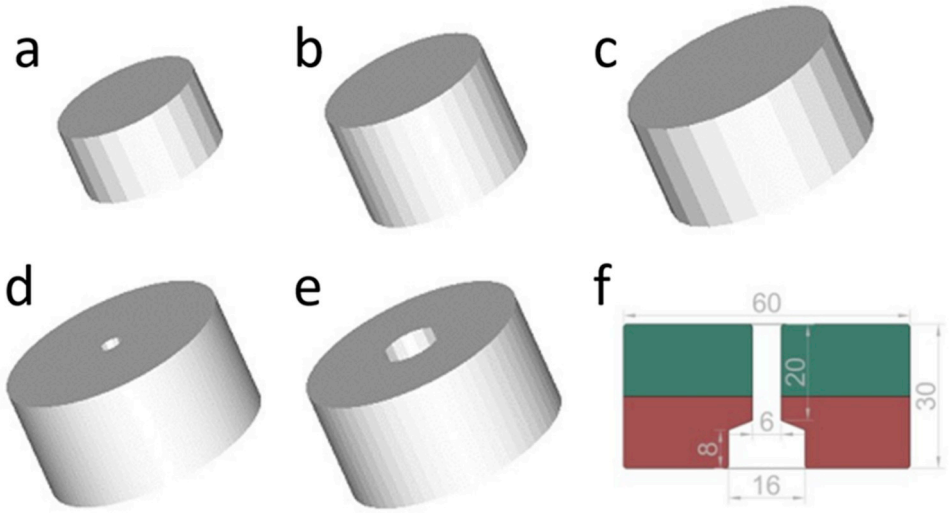

Fig. 2. The five permanent magnets used for simulations: M30 (**a**), M45 (**b**), M60 (**c**), M60qr6 (**d**), M60qr16 (**e**), cross section and dimension of M60qr (**f**).

Table 1
Characteristics of the permanent magnets used in the simulations.

Name	Diameter (mm)	Thickness (mm)	Magnetic energy stored, MGOe	Nominal strength, N (kg)
M30	30	15	42	225 (23)
M45	45	30	45	765 (78)
M60	60	30	45	1220 (120)
M60qr	60	30	45	1220 (120)

analyzed by 2D axisymmetric FEM were linearly transformed to the human head model, using an Intel Core™ i5-6500 3.20 GHz 20G-DRAM personal computer with Windows 10, in order to visualize the magnetic field distributions on the tessellated cortical surface. The center of the magnet base surfaces could thus be placed at the closest scalp node in respect to the primary motor area (M1) (see Fig. 1b). All the human head model tissues were assumed to be transparent to the static magnetic field [18].

3. Results

3.1. Magnetic flux density in the air

The mean absolute error between mean of the measured and the computed magnetic flux density values along the cylindrical axis of M60 was only 1.6%. Furthermore, the largest standard deviation among measuring points was ±4.8 mT, at axial displacement of 5 cm. Fig. 3 demonstrates comparison between measured and simulated fields. Fig. 4 shows the magnitude and gradient of the magnetic flux density at different axial and radial locations. For M60, the maximum magnitude of magnetic flux density along the central axis was 444 mT; the magnitude was reduced to 243 mT at 1.5 cm, a distance almost equal to that between the scalp surface and the cortical grey matter.

M45 produced the strongest magnetic flux density at magnet surface (504.7 mT); however, the magnetic field induced by M45 decayed at the fastest rate along the central axis. In fact, the magnitude of magnetic flux density became less than those of M60 and M60qr even before the magnetic field reached the surface of the cortical grey matter. The magnitude of the magnetic flux density induced by M30 was the smallest among all magnet types, when the axial displacement was larger or equal to 1 cm. The magnitude of the magnetic flux density induced by M60 became instead the highest when the axial displacement was larger

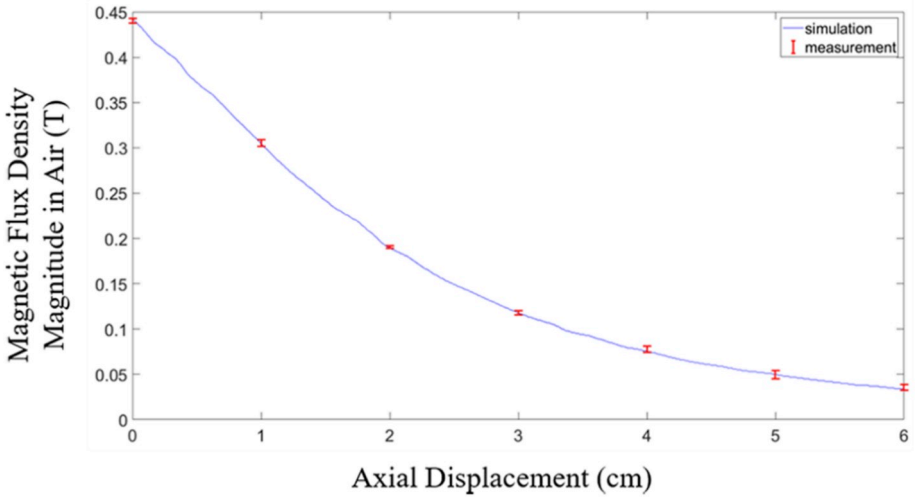

Fig. 3. Comparison of measured and simulated magnetic flux density along the cylindrical axis of M60.

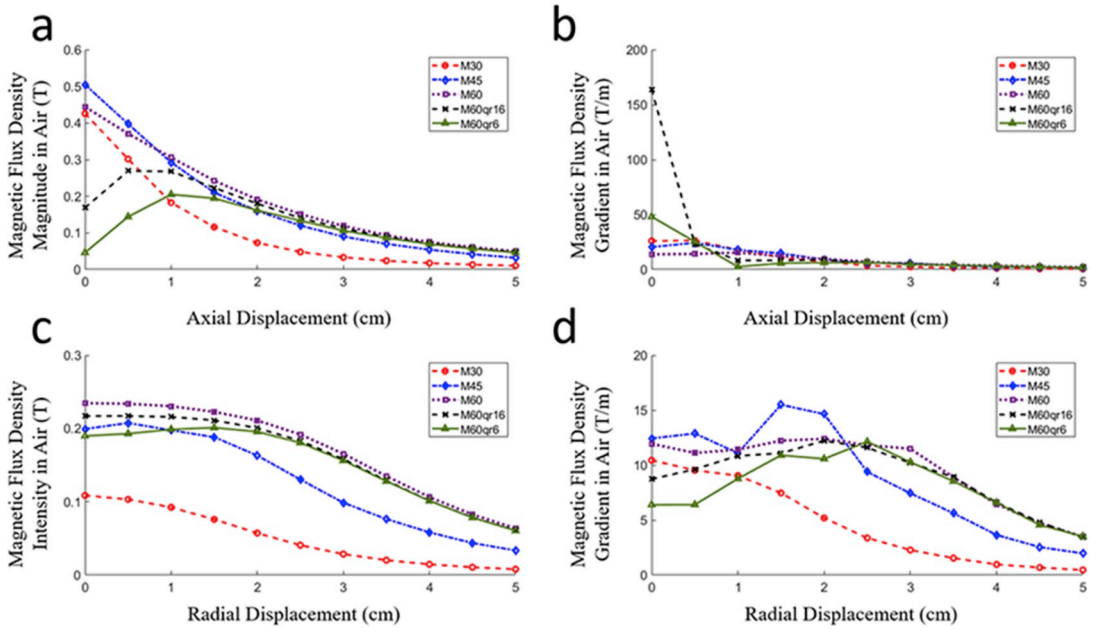

Fig. 4. Magnitude and gradient of the magnetic flux density at different spatial locations in the air: (**a**) Magnitude of the magnetic flux density along the cylindrical axis, (**b**) Gradient of the magnetic flux density along the cylindrical axis, (**c**) Magnitude of the magnetic flux density along the radial direction, and (**d**) Gradient of the magnetic flux density along the radial direction.

than 1 cm. All magnets except for M30 showed similar values in absence of radial displacement (Fig. 4c), but M45 showed the steepest decrease along the tangent of the magnet surface (radial displacement). Thus, M45 should show the most focalized magnetic field distribution on the cortical surface.

M60qr6 showed the highest field gradient at the magnet surface: its value was approximately 3.4 times greater than that of the second highest field gradient induced by M60qr16. However, the field gradient induced by M60qr6 rapidly decreased with increasing axial displacement, reaching the values of the other magnets at 1.5 cm away from the magnet base. Observations of field gradient along the radial direction showed that distance from the central axis where each magnet induced maximum field gradient varied from magnet to magnet; M60qr16 and M60 generated its maximum field gradient at 2 cm from the central axis, while M30, M45, and M60qr6 showed peaks at 0 cm, 1.5 cm, and 2.5 cm from the central axis, respectively. The local peaks of field gradient originated from the 'edge effect' [18], with anexception of M30. The highest gradient value was 15.5 T/m, induced by M45 at 1.5 cm from the central axis. All magnets showed exponential decay along the radial direction after their respective peaks.

The comparison of magnetic flux densities induced by M30, M45, and M60 around the possible cortical area (1.57 cm from the magnet base) showed that usually the larger the magnet, the greater the magnitude of the magnetic flux density (see Fig. 4c). Among the three magnets, M45 showed the highest gradient around the possible cortical area (Fig. 4d). Considering the magnetic field gradient as one of the important factors regulating the effectiveness of tSMS [2], M45 might be a good choice.

M60qr6 induced the highest peak gradient on the magnet base among all magnet types (Fig. 4b); however, as the distance from the magnet base increased, M60qr6 showed also the steepest drop in field gradient. Hence, at a distance equivalent to the distance between scalp and cortex, M60qr6 had lower gradient than the magnets without holes (Fig. 4d). M60 had the same radius and height of M60qr but induced a stronger magnetic flux density in the cortex. This suggests that magnets with holes have no advantages over the normal solid magnets.

3.2. Magnetic flux density distribution on the cortical surface of the human head model

The distributions of magnetic flux density on the cortical surface of the human head model, induced by various types of permanent magnets placed on the scalp surface, are illustrated in Figs. 5 and 6. M60 induced the strongest magnetic flux density over the cortex surface, with a peak magnitude of 244 mT. The magnetic flux density induced by M60 was 15 mT higher than that of M60qr6, which induced the second highest peak magnitude (229 mT). M30 generated the lowest peak magnitude (110 mT), but it can still be used for tSMS [16]. M45 and M60qr16 induced peak magnitudes of 214 mT and 183 mT, respectively. Those magnets inducing the strongest peak magnitudes did not necessarily induce the highest peak field gradients in the cortex (Fig. 5). M45 induced the strongest peak gradient (14.577 T/m), followed by M60 (12.766 T/m). The peak gradients of M60qr16, M30, M60qr6 were lower; they induced 9.509 T/m, 10.750 T/m, and 11.686 T/m, respectively. Interestingly, the edge effect of the field gradient (Fig. 4d) was not observed on the cortical surface, because the cortical surface was considerably curved.

While M30 induced the weakest magnetic flux density in the cortex (peak magnetic flux density = 110 mT), it could still be effective in tSMS: 38 mT is the minimum value of static magnetic field for the inhibition of miniature end plate potential (mepp) in human pyramidal cells [16]. M30 could hence be useful in the modulation of cortical excitability, for both small and local brain structures, although its stimulation intensity might be relatively weaker than those of other magnets.

4. Discussion

In this study, we simulated the spatial distributions of magnetic flux density and field gradient induced by various permanent magnets that are applicable to tSMS. Out of all the permanent magnets considered, M60 induced the highest magnetic flux density magnitude on the cortical grey matter surface, followed by M45 (Fig. 5). M60qr6 induced the strongest magnetic flux density gradient on the magnet surface; however, this gradient rapidly dropped, and even became smaller than that induced by M60 when the distance from the magnet base was larger

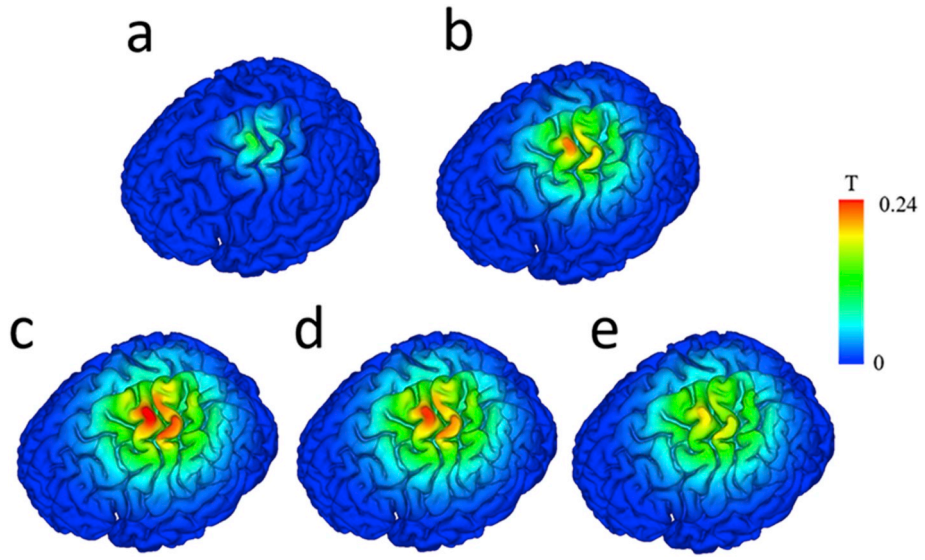

Fig. 5. Magnetic flux density induced by (**a**) M30, (**b**) M45, (**c**) M60, (**d**) M60qr6, and (**e**) M60qr16.

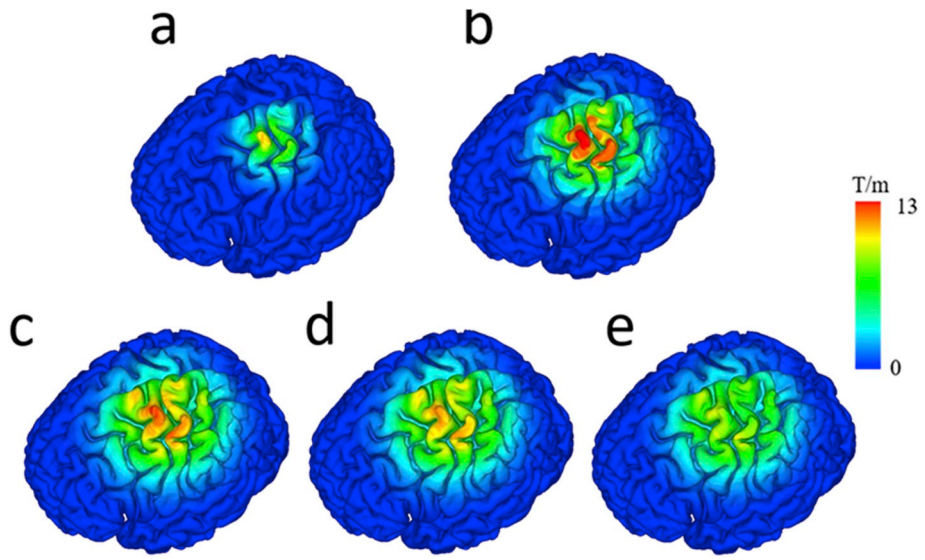

Fig. 6. Gradient of magnetic flux density induced in the cortical grey matter by (**a**) M30, (**b**) M45, (**c**) M60, (**d**) M60qr6, and (**e**) M60qr16.

or equal to 1 cm. We also concluded that magnets with a hole (i.e., M60qr in our study) might have little to no advantage over magnets without holes. Furthermore, although generally magnets with a larger volume induced higher magnetic flux density, M45 was the magnet that showed the highest peak gradient of magnetic flux density on the grey matter surface (Fig. 5). The similar tendency that magnets with larger volume do not necessarily induce higher field gradient could also be observed when the magnitude and gradient of magnetic flux density along the cylindrical axis of the magnet were evaluated using an analytic solution [21]. M45 could be advantageous if gradient plays more significant role in the mechanism of tSMS. Furthermore, the results, especially regarding gradients, may also be directly translated into other areas of application, such as magnetic drug targeting [22,23]. Finally, although M30 induced the weakest magnetic flux density and gradient, it still might be advantageous for the modulation of relatively smaller brain targets.

To compute the spatial distributions of magnetic flux density and field gradient induced by various permanent magnets, we used an axisymmetric FEM solver to analyze the spatial distributions of magnetic field quantities because all the permanent magnets employed in this study had axisymmetric shapes. As the magnetic permeability of human body was known to be the same as that of free space, the realistic human head model was not included in the analysis domain. Instead, the magnetic field distributions on the cortical surface were computed by the linear interpolation of FEM results. This approach has a potential advantage over the conventional 3D FEM approach that includes both human head and permanent magnet models in that different head models can be readily employed without any additional mesh generation process. Therefore, our approach might be useful particularly for implementing an individually-customized image-guided tSMS system that determines the optimal location and tilting angle of a permanent magnet to maximize delivery of magnetic field to specific target areas of an individual's brain.

To further confirm whether the axisymmetric FE models employed in our simulations included sufficient numbers of elements, we generated an additional FE model with fewer numbers of elements and compared the new field analysis results with our original ones. For example, the original FE model to compute magnetic fields generated by the M60

magnet included 547,012 nodes, while a newly generated FE model included only 138,408 nodes. Figs. S1(a) and S1(b) included in the Supplementary Document file shows the magnitudes of the magnetic flux density at different spatial locations. In addition, Fig. S1(c) in the Supplementary Document file shows the difference of magnetic flux density on the cortical surface. As shown in the figures, the maximum error between the two models was at most 1.7%, demonstrating that the original FE model included sufficient number of elements.

Our simulation results showed that just a slight modification in the shape of a permanent magnet (e.g., M60qr) could make a considerable difference in the spatial distributions of magnetic field quantities. The differences in magnetic field properties induced by various types of permanent magnets suggest that their careful selection, based on magnetic field simulations, might be necessary to increase the effectiveness of tSMS. In the future, evaluation of more permanent magnet types would be necessary to find the optimal permanent magnet that generally maximizes the outcomes of tSMS.

Besides the five permanent magnet types simulated in this study, we newly simulated two magnets that are commercially available but have never been used for tSMS. The two permanent magnets are M35 and M70, both of which are manufactured by Supermagnete (Gottmadingen, Germany), a distributor of permanent magnets considered in this study except M60. Dimensions of the two magnets are provided in Table S1 and Fig. S2 of Supplementary Document file attached to this manuscript. The magnitude and gradient of magnetic flux density of these two magnets were evaluated either along some designated axes or on the cortical surface, and the simulation results are shown in Figs. S3, S4, and S5 included in the Supplementary Document file, where the magnetic fields generated by M35 and M70 were compared with those generated by M45 and M60. Note that Figs. S3, S4, and S5 correspond to Figs. 4–6, respectively. It could be observed from Fig. S3 that M70 did not produce the strongest magnetic flux density at the center of magnet surface (Fig. S3a); however, it produced highest magnetic flux density of 260 mT at 1.5 cm above the magnet surface (Fig. S3c). M35 produced the highest field gradient of 22.6 T/m at the center of magnet surface (Fig. S3b); however, since M35 produced the weakest magnetic flux density at 1.5 cm above the magnet surface (Fig. S3c). Along an axis parallel to the magnet surface with the distance from the surface being 1.5 cm, M70 showed its maximal field gradient at the radial displacement of 3 cm (12.2 T/m), whereas M35 peaked on the cylindrical axis (11.5 T/m). However, the maximal gradient values of both M70 and M35 magnets were smaller than that of M45 (Fig. S3d). M45 was still the magnet that showed the highest peak gradient of magnetic flux density on the grey matter surface (Fig. S5). The M35 magnet did not exhibit impressive performance in terms of both field strength and gradient; however, M70 can be considered as a good alternative of M60 because M70 showed stronger magnetic flux density than M60 and showed similar field gradient profile to M60.

Despite some recent cellular-level investigations on tSMS [2,24], the mechanisms behind tSMS are still largely unknown; hence, the comparison of behavioral and physiological outcomes using different permanent magnets might be an interesting topic for future research. In addition, the use of non-cylindrical magnets might enhance the overall efficacy of tSMS. Of course, a full-3D FEM needs to be employed to simulate such non-cylindrical permanent magnets, which is related to a limitation of our study. Furthermore, individual customization of stimulation parameters such as locations and orientations of permanent magnets might also enhance the efficacy of tSMS. Indeed, there exist large inter-individual variability in the structure of the human brain, e.g., cortical sulcal depth, size of the brain, and skull thickness. It is expected that the simulation protocols employed in this study would be used for the individually customized tSMS. In the future it would also be interesting to compare variations of magnetic field properties between multiple subjects or cortical regions, or use multiple permanent magnets simultaneously and/or design special-shape magnets (e.g., Halbach arrays) to create a more focalized field distribution over the human cerebral cortex.

5. Conclusion

Distinct advantage of tSMS over other noninvasive brain stimulation techniques, such as tDCS and TMS, is that its working mechanism does not involve electric fields, thereby being free from side effects associated with electric fields. Although there is a clear limitation of tSMS in that facilitation of brain activity is not possible, tSMS can be a cheap alternative to inhibitory protocols of TMS and cathodal tDCS. To further popularize tSMS in practical applications, developing methods to "shape" magnetic fields for better focality is desired. This work aims at probing magnetic field properties of various permanent magnets on human cortical grey matter. Our results showed that moderate change in the shape of a permanent magnet significantly reduces the spatial distributions of magnetic field quantities. Furthermore, it was shown that using magnets with a hole may be disadvantageous. Additionally, it was observed that magnetic flux density was proportional to the volume of permanent magnet, but its gradient was not. In summary, different magnetic field properties induced by various types of permanent magnets suggest that the permanent magnets for tSMS need to be carefully selected based on the refined magnetic field simulation to increase the effectiveness of tSMS.

Conflict of Interest Statements

There are no conflicts of interest to declare.

Acknowledgements

This work was supported in part by the National Research Foundation of Korea grants funded by Ministry of Science, ICT & Future Planning (NRF-2015M3C7A1031969 & 2019M3C7A1031278), and in part by a grant of Korea Health Technology R&D Project through the Korea Health Industry Development Institute, funded by the Ministry of Health and Welfare, Republic of Korea (HI17C1501).

Appendix A. Supplementary data

Supplementary data to this article can be found online at https://doi.org/10.1016/j.compbiomed.2019.103476.

References

[1] A. Oliviero, L. Mordillo-Mateos, P. Arias, I. Panyavin, G. Foffani, J. Aguilar, Transcranial static magnetic field stimulation of the human motor cortex, J. Physiol. 589 (Pt 20) (2011) 4949–4958.
[2] M.J. McLean, S. Engstrom, Z. Qinkun, C. Spankovich, D.B. Polley, Effects of a static magnetic field on audiogenic seizures in black Swiss mice, Epilepsy Res. 80 (2–3) (2008) 119–131.
[3] I.D. Milovanovich, et al., Homogeneous static magnetic field of different orientation induces biological changes in subacutely exposed mice, Environ. Sci. Pollut. Res. Int. 23 (2) (2016) 1584–1597.
[4] K. Nakagawa, A. Sasaki, K. Nakazawa, Accuracy in pinch force control can be altered by static magnetic field stimulation over the primary motor cortex, Neuromodulation: Technol. Neural Interface (2019), https://doi.org/10.1111/ner.12912.
[5] A. Lacroix, L. Proulx-Bégin, R. Hamel, L. De Beaumont, P.-M. Bernier, J.F. Lepage, Static magnetic stimulation of the primary motor cortex impairs online but not offline motor sequence learning 9 (1) (2019) 9886.
[6] H. Kirimoto, A. Asao, H. Tamaki, H. Onishi, Non-invasive modulation of somatosensory evoked potentials by the application of static magnetic fields over the primary and supplementary motor cortices, Sci. Rep. 6 (2016) 34509.
[7] J.J. Gonzalez-Rosa, et al., Static magnetic field stimulation over the visual cortex increases alpha oscillations and slows visual search in humans, J. Neurosci. 35 (24) (2015) 9182–9193.
[8] J. Aguila, J. Cudeiro, C. Rivadulla, Effects of static magnetic fields on the visual cortex: reversible visual deficits and reduction of neuronal activity, Cerebr. Cortex 26 (2) (2016) 628–638.
[9] H. Kirimoto, et al., Effect of transcranial static magnetic field stimulation over the sensorimotor cortex on somatosensory evoked potentials in humans, Brain Stimul 7 (6) (2014) 836–840.

[10] C. Carrasco-Lopez, et al., Static magnetic field stimulation over parietal cortex enhances somatosensory detection in humans, J. Neurosci. 37 (14) (2017) 3840–3847.
[11] K. Heimrath, A. Spröggel, S. Repplinger, H.J. Heinze, T. Zaehle, Transcranial Static Magnetic Field Stimulation over the Temporal Cortex Modulating the Right Ear Advantage in Dichotic Listening, Neuromodulation: Technol. Neural Interface. 10 (5) (2019) e0127061.
[12] A. Matsugi, Y.J. F.n. Okada, Cerebellar transcranial static magnetic field stimulation transiently reduces cerebellar brain inhibition 32 (2) (2017) 77.
[13] C. Rivadulla, G. Foffani, and A. Oliviero, "Magnetic field strength and reproducibility of neodymium magnets useful for transcranial static magnetic field stimulation of the human cortex," Neuromodulation, vol. 17, no. 5, pp. 438-441; discussion 441-2, Jul 2014.
[14] A. Oliviero, et al., Safety study of transcranial static magnetic field stimulation (tSMS) of the human cortex 8 (3) (2015) 481–485.
[15] M. Dileone, L. Mordillo-Mateos, A. Oliviero, G. Foffani, Long-lasting effects of transcranial static magnetic field stimulation on motor cortex excitability, Brain Stimul 11 (4) (2018) 676–688.
[16] A.D. Rosen and biophysics, Mechanism of action of moderate-intensity static magnetic fields on biological systems 39 (2) (2003) 163–173.
[17] P. Davila-Pérez, A. Pascual-Leone, J.J.N. Cudeiro, Effects of transcranial static magnetic stimulation on motor cortex evaluated by different TMS waveforms and current directions 413 (2019) 22–30.
[18] J.J. Tharayil, S.M. Goetz, J.M. Bernabei, A.V. Peterchev, Field distribution of transcranial static magnetic stimulation in realistic human head model, Neuromodulation 21 (4) (2018) 340–347.
[19] M. Windhoff, A. Opitz, A. Thielscher, Electric field calculations in brain stimulation based on finite elements: an optimized processing pipeline for the generation and usage of accurate individual head models, Hum. Brain Mapp. 34 (4) (2013) 923–935.
[20] D. Meeker, "Manual of Femm4. vol. 2," ed.
[21] J. Camacho, V. Sosa, Alternative method to calculate the magnetic field of permanent magnets with azimuthal symmetry 59 (1) (2013) 8–17.
[22] S.J.F. Kenjereš, On recent progress in modelling and simulations of multi-scale transfer of mass, momentum and particles in bio-medical applications, Flow, Turbul. Combust. 96 (3) (2016) 837–860.
[23] S. Kenjereš, B.W. Righolt, F. Flow, Simulations of magnetic capturing of drug carriers in the brain vascular system 35 (2012) 68–75.
[24] A. Cavopol, A. Wamil, R. Holcomb, M.J.B. McLean, Measurement and analysis of static magnetic fields that block action potentials in cultured neurons 16 (3) (1995) 197–206.